HHS Public Access

Author manuscript

Ultrasound Med Biol. Author manuscript; available in PMC 2020 January 01.

Published in final edited form as:

Ultrasound Med Biol. 2019 January ; 45(1): 137–147. doi:10.1016/j.ultrasmedbio.2018.09.006.

BOILING HISTOTRIPSY ABLATION OF RENAL CELL CARCINOMA IN THE EKER RAT PROMOTES A SYSTEMIC INFLAMMATORY RESPONSE

George R. Schade[a], **Yak-Nam Wang**[b], **Samantha D'Andrea**[c], **Joo Ha Hwang**[c], **W. Conrad Liles**[c], and **Tatiana D. Khokhlova**[c]

[a]Department of Urology, University of Washington, Seattle, WA 98195

[b]Center for Industrial and Medical Ultrasound, Applied Physics Lab, University of Washington, Seattle, WA 98105

[c]Department of Medicine, University of Washington, Seattle, WA 98195

Abstract

Boiling histotripsy (BH) is an experimental focused ultrasound technique that produces non-thermal mechanical ablation. We evaluated the feasibility, short-term histologic effects, and the resulting acute inflammatory response to BH ablation of renal cell carcinoma (RCC) in the Eker rat. Genotyped Eker rats were monitored for *de novo* RCCs with serial ultrasound (US) imaging. When tumors were ≥8 mm, rats underwent ultrasound-guided extracorporeal ablation of the tumor with BH, a pulsed focused US technique that produces non-thermal mechanical ablation of targeted tissues, or a sham US procedure. Treatments targeted approximately 50% of the largest RCC with a margin of normal kidney. BH treated rats were euthanized at 1 (n=4) or 48 (n=4) hours, and sham subjects (n=4) at 48 hours. Circulating plasma cytokine levels were assessed with multiplex assays prior to and at 0.25, 1, 4, 24 and 48 hours following treatment. Kidneys were collected and processed for histologic assessment, immunohistochemistry and intrarenal cytokine concentration measurements. For statistical analysis Student's t-test was used. US-guided BH treatment was successful in all animals, producing hypoechoic regions within the targeted volume consistent with BH treatment effect. Grossly, regions of homogenized tissue were apparent with evidence of focal intra-parenchymal hemorrhage. Histologically, BH produced a sharply demarcated region of homogenized tumor and non-tumor tissue containing acellular debris. BH treatment was associated with significantly increased relative concentration of plasma TNF vs. sham treatment ($p<0.05$) and transient elevations in HMGB1, IL-10 and IL-6 consistent with acute inflammatory response to trauma. Intrarenal cytokine concentrations followed the same trend. At 48 hours, enhanced infiltration of $CD8^+$ T cells was observed by immunohistochemistry in both the treated and un-treated contralateral RCC/kidneys in BH-treated animals vs. sham treatment. BH treatment was well tolerated with transient gross hematuria and a perinephric hematoma developing in one subject each. The study demonstrates the feasibility of BH ablation of *de novo* RCC and suggests activation of the acute inflammatory cascade following treatment that appears

Corresponding Author: Tatiana D. Khokhlova, Box 359773, 325 Ninth Avenue, Seattle, WA 98104, phone: 206-543-6193, tdk7@uw.edu.

to stimulate CD8+ T cell infiltration of both treated and untreated tumors. Longer duration chronic studies are ongoing to characterize the longevity and robustness of this response.

Keywords

Renal Carcinoma; Kidney Cancer; Histotripsy; FUS; HIFU; Immune Response; T-Cells

INTRODUCTION

Histotripsy is a pulsed focused ultrasound (FUS) technique that produces non-thermal mechanical homogenization of targeted tissue (Khokhlova et al. 2015). As initially described, histotripsy involves delivery of short (less than 20 microseconds) high intensity pulses of FUS to induce formation of microbubbles in targeted tissue via acoustic cavitation (Hall et al. 2009, Parsons et al. 2006). Subsequent oscillation and collapse of these bubbles produce mechanical fractionation of targeted tissues, while enabling real-time ultrasound (US) guidance due to the high reflectivity of bubbles. The feasibility of using this “cavitation cloud” histotripsy technique to ablate a variety of benign and malignant tissues has been demonstrated, leading to Phase 1 clinical studies for benign urologic applications. We have been developing an alternative approach to histotripsy, in which longer (1–10 ms), but lower amplitude FUS pulses are utilized to form vapor bubbles within a few milliseconds at the focus in a process that involves efficient shock-wave heating (Khokhlova et al. 2011). Interaction of the vapor bubbles with the pulses produces acoustic fountaining that in turn mechanically disrupts cells into a homogenate of subcellular debris with negligible thermal effects (Simon et al. 2012). This technique, termed boiling histotripsy (BH), circumvents the stringent size and output power requirements of cavitation cloud histotripsy therapy transducers, while achieving the same mechanically mediated tissue effects.

Previous *ex vivo* and *in vivo* studies have demonstrated the ability to achieve precise mechanical ablation of a variety of soft tissues with BH, including kidney (Hoogenboom et al. 2016, Khokhlova et al. 2014, Khokhlova et al. 2016). Based on these results, we hypothesize that BH can be developed into an effective, non-invasive treatment of renal cell carcinoma (RCC). To date, clinical management of RCC is stage dependent. For patients presenting with small (<4 cm) renal masses nephron sparing surgery with a partial nephrectomy is the current gold standard treatment (Campbell et al. 2009). While efficacious (5 year local recurrence free survival rate of ~98%), partial nephrectomy is not without inherent risks and morbidity with complication rates up to 24%, including bleeding, urinary fistula, and conversion to radical nephrectomy (Klatte et al. 2011). In an effort to minimize periprocedure morbidity, focal therapies, including radiofrequency ablation and cryotherapy, have been adopted for select RCC patients. However, these ablative therapies have several limitations with respect to their invasiveness, the location, shape and size of tumors that can be treated, and the limited real-time treatment monitoring and feedback they offer (Venkatesan et al. 2011). Specifically, the ideal renal tumor for these percutaneous thermal therapies is a peripheral, regularly shaped tumor <3 cm in size due to the reliance on thermal diffusion and the time required to achieve the desired “kill” temperature. Owing to the limitations outlined above, thermal ablation has been limited to tumors smaller than 4 cm

and has been associated with increased local recurrence rate of up to 10% (Campbell et al. 2009). As a result, there is a need for more efficacious and less invasive ablative therapy. BH has the potential to overcome many of the challenges facing other ablative therapies due to its non-invasive delivery that does not rely on thermal diffusion to achieve the effect and can therefore potentially treat larger, irregularly shaped tumors, in close proximity to the renal sinus and other critical structures.

Recent pre-clinical studies have indicated that mechanical tumor ablation or lysis through cryotherapy or mechanical HIFU may enhance systemic anti-tumor immune response through release of large quantities of tumor antigens, that are not thermally denatured, along with endogenous danger-associated molecular pattern signals (DAMPs or alarmins) from lysed tumor cells *in situ* (den Brok et al. 2006, Hu et al. 2007). The rapid release of alarmins from necrotic or damaged cells initiates cytokine cascades that lead to recruitment and activation of effector cells of the innate immune system that can subsequently promote activation of adaptive immune responses (Chan et al. 2012, Chen and Nunez 2010). When taken in the context of the well-defined immune aberrations in RCC and increasing role of immunotherapy in metastatic RCC (Draube et al. 2011, McDermott et al. 2015), we hypothesize that mechanical RCC ablation by BH may provide additional systemic therapeutic benefits for patients with localized disease while serving as part of a more efficient systemic immunotherapy for patients with metastatic disease.

The two major goals of this work were to demonstrate the feasibility of *in vivo* BH renal tumor ablation in a *de novo* hereditary small animal RCC model and to perform an initial exploration of the ensuing inflammatory response in terms of changes in tumor infiltrating lymphocytes and cytokine milieu.

MATERIALS AND METHODS

Tumor model

The Eker rat RCC model was used due to its spontaneous tumor development, similar tumor morphology and biology compared to human RCC, and intact immune system. Eker rats inherit an autosomal dominant point mutation in the tumor suppressor gene *Tsc2*. Subsequent loss of the other *Tsc2* allele produces RCC, often bilateral and of variable histology, in ~100% of heterozygous (*Tsc2+/−*) animals by 12 months (McDorman et al. 2002). Although the inciting event is loss of *Tsc2*, as opposed to VHL in humans, Eker rat renal tumorigenesis is characterized by a similar hypoxia-like phenotype with accumulation of HIF-2α, overexpression of VEGF and neovascularity (Liu et al. 2003). Additionally, Eker rat RCCs are characterized by increased mammalian target of rapamycin (MTOR) signaling (Habib 2011, Kenerson 2002) with MTOR inhibition suppressing tumor growth. From an immune standpoint, Eker rats with large tumor burden have decreased cellular and humoral immunity compared to non-tumor bearing syngeneic rats, similar to immune alterations seen in human RCC (Waynforth et al. 1981).

After obtaining approval from the University of Washington Institutional Animal Care and Use Committee, genotyped Eker rats (*Tsc2* heterozygotes) underwent monthly bilateral renal US imaging under isoflurane anesthesia (5% induction, 2% maintenance) using a high

frequency ultrasound imaging probe (L7–18 linear array, center frequency 12 MHz, , Alpinion Medical Systems, Seoul, Korea) to assess tumor burden beginning at nine months. When the largest RCC was ≥8 mm (10–14 months old) rats were randomly assigned to treatment with BH or a sham procedure.

Boiling histotripsy setup and treatment

BH treatment was performed using a customized pre-clinical FUS system (VIFU-2000, Alpinion Medical Systems, Bothell, WA, USA) (Figure 1). A 1.5 MHz single-element, spherically-focused transducer (64 mm aperture, 45 mm radius of curvature, focus size at −6 dB level 7.5 mm × 0.8 mm × 0.8mm in linear propagation regime) was mounted in a water bath filled with degassed water and maintained at 37°C and powered by a computer-controlled function generator/amplifier. The FUS transducer was fitted with an ultrasound-imaging probe (C4–12 phased array, center frequency: 7 MHz) via a central opening for in-line treatment planning and monitoring. The transducer focus location was preregistered and indicated on the US monitor.

Prior to BH treatment, each animal was anesthetized by isoflurane inhalation and maintained in surgical plane of anesthesia. The ipsilateral flank was shaved and depilated for acoustic coupling. High-resolution US imaging (L7–18 linear array, center frequency 12 MHz, Alpinion Medical Systems, Seoul, Korea) was performed to confirm tumor location and dimensions. After a pretreatment blood draw from the tail vein, the animal was positioned in a custom-built holder, that was attached to a computer-controlled 3D positioning system, and submerged in the water tank for treatment planning. The transducer focus was aligned with the center of the tumor. The BH treatment plan was then generated to cover 50% of the tumor region using a grid of treatment foci spaced by 1 mm in the vertical and horizontal planes (8–20 focal points overall, depending on the tumor size). Only ~50% of the tumor volume was targeted to allow confirmation of successful targeting of the intended tumor and assessment of leukocyte infiltrates into the remaining tumor tissue. During BH treatment, the animal holder was moved in a raster pattern to deliver the planned treatment foci. The transient appearance of bright hyperechoic bubbles near the focus with each BH pulse (Figure 1b and Supplementary Video 1) provided real-time visualization of the tumor area being treated and feedback as to whether the *in situ* focal pressures were sufficient to produce BH. Gradual loss of structure in the treated area manifested itself as the appearance of hypoechoic region containing swirls of transient bubbles, that allowed to evaluate treatment progress. Sham animals underwent the same procedures, except the FUS transducer was not turned on while the imaging US transducer was raster-scanned through the tumor.

Ten pulses of 10 ms duration, at pulse repetition frequency of 1 Hz were delivered to each focal spot, at an electric power of 525 – 575W, depending on the tumor depth. The power level was adjusted within that range based on the observation of the hyperechoic region at the focus. The peak focal pressure levels corresponding to these output levels were previously measured in water by fiber optic probe hydrophone (FOPH-2000, RP Acoustics, Leutenbach, Germany) as follows: peak positive pressure 90–100 MPa, peak negative pressures 17–20 MPa, shock amplitudes 85–100 MPa. This pulsing sequence was devised

and used in our prior work for BH liquefaction of subcutaneously grafted prostate cancer tumors in rats (Chevillet *et al.* 2017). In addition, preliminary BH exposures in *ex-vivo* rat kidney were conducted prior to the start of the study to optimize spacing of the focal spots and the number of BH pulses delivered per spot. A single BH cavity produced by delivering 10 pulses was nearly elliptical in shape and 2 mm × 2 mm × 7 mm in size, and the cavities would merge into continuous liquefied volume if spaced 1 mm apart.

Post-treatment care and sample collection

A schematic of the procedure timeline is illustrated in Figure 1c. Immediately after treatment, rats were removed from the holder and placed on a warming pad. Post-treatment blood withdrawals were performed 10 min, 1 hour, 6 hours, 24 hours, and 48 hours after treatment. High resolution US imaging of the treated kidney was performed immediately following each blood withdrawal to evaluate the treated RCC for changes in echotexture (i.e., the lesion). Following the 1 hour time point, rats were emerged from anesthesia and were then briefly re-anesthetized for subsequent blood draws and imaging. For analgesia, rats received subcutaneous ketoprofen (10 mg/kg) 1 hour and 24 hours post-treatment and subcutaneous saline (10 ml/kg) for volume resuscitation following the 1 hour blood draw. All blood samples were transferred to EDTA-coated tubes immediately following collection, centrifuged for 5 minutes at RCF=800, and plasma was aspirated and immediately frozen and stored at −80°C for subsequent cytokine assays. Rats were euthanized at 1 hour (BH treated n=4) and 48 hours (BH treated n=4, sham treated n=4) via anesthesia overdose and terminal blood draw. Necropsy was performed to evaluate for gross complications, and both kidneys were removed, grossly inspected, and photographed. A 3-mm punch biopsy was taken adjacent to the BH-treated or sham-treated RCC (to allow for undisturbed histologic assessment of BH treatment) and frozen for subsequent intrarenal cytokine assay. The kidneys were embedded in optimum cutting temperature medium (Tissue Tek, Sakura, Japan) for histological analysis and immunohistochemistry (IHC).

Cytokine assays

Prior to performing cytokine assays, the kidney tissue cores were weighed (the weight ranged within 20–90 μg, depending on the thickness of the kidney), thawed and homogenized in lysis buffer (MSD Tris lysis buffer with Inhibitor Pack, Mesoscale Diagnostics, Rockville, MD, USA) using a small dounce homogenizer. The homogenate was centrifuged at RCF=20,000 for 10 minutes, and supernatant collected. Total protein concentration in the kidney tissue lysates was determined using the Bradford protein assay (Thermo Fisher Scientific, Waltham, MA, USA) for subsequent normalization of the cytokine concentration. Cytokine concentrations in plasma samples and renal tissue lysates were evaluated with a multiplex assay (V-plex proinflammatory panel 2, Mesoscale Diagnostics, Mesoscale Diagnostics, Rockville, MD, USA) targeting rat IFN-γ, IL-10, IL-13, IL-1β, IL-4, IL-5, IL-6, IL-8 and TNF per manufacturer's protocol. A separate multiplex assay was used to measure IL-1α concentrations (Rat IL-1α Ultra-Sensitive Kit, Mesoscale Diagnostics, Mesoscale Diagnostics, Rockville, MD, USA). The multiplex plates were read on MSD Sector S 600 instrument and analyzed with Discovery Workbench assay analysis. The concentration of the alarmin HMGB-1 was measured in plasma samples using a commercially available ELISA kit (HMGB1 ELISA Kit II, Shino-test corporation, Japan).

All assays were performed in duplicates. Cytokine levels were normalized to the pre-treatment level, due to high inter-subject variability of pre-treatment cytokine levels, and were compared with Student's T-test.

Histology and immunohistochemistry

For each subject, serial 4 micron-thick frozen sections were taken from both the BH or sham treated tumor/kidney and contralateral kidney. Serial sections were then stained with hematoxylin and eosin (H&E) to visualize tissue structure, underwent nicotinamide adenine dinucleotide diaphorase (NADH-d) staining as previously described (Wang et al. 2013, Khokhlova et al. 2014) to confirm absence of thermal damage, or processed for immunohistochemistry (IHC). IHC was performed using a Leica Bond Max automated stainer (Leica Biosystems, Buffalo Grove, IL, USA) using a standard protocol. The primary antibodies used to characterize infiltration by T cells included: CD8 (1:2000, 15-11C5, Hycultbiotech), CD4 (1:500, W3/25, Abdserotec) and FoxP3 (1:100, mAbcam 22510, Abcam); macrophages and dendritic cells: F4/80 (1:500, ab74383, Abcam), CD163 (1:500, ED2, Abdserotec), and CD11c (1:100, Abcam); and neutrophils: myeloperoxidase (MPO, Thermofisher Scientific). In addition, alterations in renal parenchymal and tumor cellular proliferation following treatment were assessed by staining for Ki67 (1:100, PA-516446, Thermofisher Scientific). All slides were stained using previously optimized conditions including a positive control (rat spleen) and a non-primary antibody control. IHC reaction was detected using the Leica Bond Polymer Refine detection kit (Leica Biosystems) and 3,3'-diaminobenzidine tetrahydrochloride (DAB) was used as a chromogen. Hematoxylin was used as the counterstain.

RESULTS

Boiling histotripsy treatment effects

BH treatment produced transient hyperechoic bubbles readily observable on US imaging at the focus with each treatment pulse. As treatment progressed, loss of targeted tissue structure became apparent as a hypoechic cavity (between pulses). On high resolution US imaging immediately after BH, a heterogenous hypoechoic cavity persisted (Figure 2). The treatment was generally well tolerated, with no rats requiring analgesia beyond 24 hours post-treatment and exhibiting no outward signs of pain. All rats were active and observed eating within 24 hours. Transient (<24 hrs) hematuria was observed in one BH treated rat in which the tumor was centrally located. At necropsy, an asymptomatic perinephric hematoma was observed in one BH treated rat that survived for 48 hours. No collateral injury to surrounding tissues was observed grossly. Representative gross images of tumor bearing kidneys from BH and sham-treated rats are shown in Figure 3a. As expected, sham-treated kidneys appeared normal with spheroid tumors. Inspection of kidneys/tumors 1 hour after BH demonstrated petechial and/or subcapsular blood consistent with mechanical trauma. At the 48-hour time point, the kidney appeared mildly edematous with petechial blood, and the BH-liquefied region clearly visible as a dark subcapsular region.

Histological appearance of sham and BH treated RCC is presented in Figure 3. Sham treatment produced no observable histologic effects. Conversely, BH treatment produced

homogenized tumor and renal parenchyma confined to the targeted region 1 hour post-treatment. There was sharp demarcation between treated and intact tissue with a transition zone 1–2 cells wide. The homogenized area contained sub-micron cell debris and occasional intact cell nuclei, with no intact tumor or parenchymal cells. Additionally, focal intact erythrocytes were seen within the ablation cavity suggestive of mild hemorrhage. Normal NADH-d staining of both the fractionated and adjacent intact tumor/parenchyma confirmed no observable thermal damage (see Supplemental Figure 1). At 48-hours post-treatment, BH-treated regions appeared similar with near absence of discernable cellular structures and persistent sharp boundaries between viable and treated tumor/parenchyma. Small areas of focal hemorrhage within the lesion and non-disrupted immediately adjacent tumor/parenchyma (within 200–500 microns) were similarly observed. Additionally, significant inflammatory infiltrates were observed at the BH lesion border and adjacent tumor/parenchyma.

Representative IHC sections of Ki67-stained 48-hour kidneys are presented in Figure 4. Normal renal parenchyma immediately adjacent to the BH cavity (within a 0.5–1 mm border) exhibited increased intense positive nuclear Ki67 staining indicating enhanced proliferation and tissue repair. ConverselRCC immediately adjacent to the BH cavity demonstrated unchanged Ki-67 staining vs. other regions in the same tumor, distant ipsilateral or contralateral tumors, or sham-treated control tumor. This suggested that BH treatment did not stimulate proliferation of remaining RCC.

Boiling histotripsy immune effects

Cytokine assays: Temporal trends in circulating plasma HMGB1 and cytokines after BH or sham treatment are shown in Figure 5. All levels were normalized to the pre-treatment level due to high inter-subject variability of the initial cytokine levels. Plasma levels of HMGB1 increased immediately (within 15 minutes), peaked around 4 hours, and then returned to baseline by 48 hours post BH treatment vs. sham treatment, although these changes did not reach statistical significance. Similarly, plasma TNF levels increased rapidly following BH treatment, but not sham treatment, reaching statistical significance at 15 minutes and 4 hours ($p=0.022$ and $p=0.043$, respectively) and then converging by 48 hours. Evaluation of plasma IL-6 and IL-10 revealed similar relationships, with IL-6 demonstrating a trend toward increased plasma levels following BH treatment within 1–24 hours and IL-10 demonstrating a slower rise in the first 48 hours post-treatment. No trends were observed in plasma levels in any of the other cytokines analyzed (IL-1α and β, IL-5, IL-8 and IL-13, Supplemental Figure 2).

Intrarenal cytokine levels from BH-treated, sham-treated, and contralateral kidneys are presented in Figure 6. Cytokine levels were compared between BH and sham-treated controls and between their respective contralateral kidneys separately. BH-treatment was associated with significantly higher intra-renal IL-10 ($p=0.03$) and significantly lower IFN-γ vs. sham-treatment 48 hours after treatment in the treated kidneys. Additionally, there was a non-significant trend toward increased 48-hour intrarenal TNF, IL-6, IL-8 and IL-13 in BH-treated vs sham-treated kidneys. Contralateral kidneys demonstrated similar non-significant trends for IL-10, IL-6, and IL-8 at 48 hours.

Immunohistochemistry: Figure 7 shows representative histological kidney sections stained for CD8+ T-cells in BH-treated RCC, contralateral RCC in the same animal, and sham-treated RCC. Very few infiltrating CD8+ T-cells were seen in sham-treated RCCs and the surrounding kidney parenchyma. Conversely, enhanced CD-8+ T-cell infiltration was observed in BH-treated tumor, including the fractionated and intact portions, as well as adjacent normal parenchyma. Interestingly, increased CD8+ T-cell infiltration was also observed in the contralateral kidneys of BH-treated rats vs. sham-treated rats, albeit to a lesser extent. These observations were consistently observed in all BH-treated animals (but not sham control animals) at 48 hour post-treatment.

No appreciable differences were observed between BH or sham treatment in the IHC tissue sections stained for M1 and M2 macrophages (F4/80 and CD163 respectively) or CD4+ T-cells. Little to no positive staining was observed in any of the IHC sections stained for dendritic cells (CD11c), FoxP3 and neutrophils (MPO) (Supplementary Figure3).

Discussion

We investigated the feasibility of non-invasive BH mechanical ablation of RCC and the resulting acute immune response to treatment in the Eker rat model. BH treatment was successful in all animals, producing the expected precise homogenization of targeted tumor and renal parenchyma. Importantly, BH ablation was associated with measurable changes in the immune system immediately after and for up to 48 hours following treatment. Specifically, we observed near immediate, transient release of the DAMP/alarmin HMGB-1 into the plasma, which appeared to trigger an inflammatory cascade, as evidenced by the measured alterations in the plasma and intra-renal cytokine milieu (Klune et al. 2008). Further, BH treatment was associated with increased infiltration of CD-8+ T-cells into not only the BH-treated RCC but also contralateral untreated RCC at 48 hours post-treatment, indicating the initiation of systemic adaptive immune response.

BH treatment was generally well tolerated in all subjects up to 48 hours, and did not require analgesia beyond the 24-hour time point. These observations are encouraging and hint at the safety and tolerability of developing BH into a non-invasive, potentially outpatient, procedure for RCC. Further larger animal preclinical studies are needed to confirm these findings. While BH was well-tolerated, we did observe minor bleeding complications (N=1 each: perinephric hematoma and hematuria) in this small animal model. While this will require further evaluation in larger animal models, we anticipate that the risk of bleeding will be reduced in larger animals and humans due to the larger caliber of renal blood vessels (>100 μm). Previously, we have shown such vessels to be very resistant to BH-induced mechanical damage, and that disrupted smaller capillaries clotted before they could cause extensive bleeding (Khokhlova et al. 2014, Khokhlova et al. 2016). Another important concern in any ablative treatment is whether incomplete ablation may cause enhanced proliferation of residual tumor cells as has been observed in incompletely thermally ablated Renca tumors in mice within hours (Kroeze et al 2012). Ki67 staining results in this study indicated that BH ablation did not enhance the proliferation of remaining Eker RCC tissue within 48 hours post-treatment. Conversely, benign renal parenchyma highly expressed

Ki-67 in a narrow rim adjacent to the BH cavity, consistent with proliferation of endogenous epithelial cells involved in tissue repair after renal injury (Humphreys et al. 2008).

It has been previously suggested by preclinical and clinical studies that mechanical disruption of tumor by FUS (Huang et al. 2012, Xing et al. 2008) may enhance systemic anti-tumor immune responses and cause anti-tumor effects in distant sites. The current understanding of the mechanism of this response is that pro-inflammatory cytokine milieu induced by the treatment promotes the recruitment of antigen-presenting cells (dendritic cells and macrophages) to the treated tumor site. The availability of previously unexposed, un-denatured intracellular tumor antigens at the treated site leads to antigen uptake and maturation of the antigen-presenting cells. Subsequent cross-presentation to naïve CD8+ cytotoxic T-cells in the lymph nodes causes their activation, proliferation and infiltration of the distant tumor sites. In the present study, we examined the short-term (up to 48 hours) dynamics of the cytokine milieu following tumor liquefaction by BH and the populations of tumor-infiltrating white blood cells at the 48-hour time point. While these measurements did not directly confirm all aspects of the immune response mechanism (e.g. we did not aim to identify specific tumor antigens responsible for T cell activation, nor did we document the process of cross-presentation), they did provide evidence for BH-triggered systemic innate and adaptive immune responses, as well as the evaluation of temporal dynamics of these responses.

At the systemic level, the cytokine milieu was characteristic of sterile inflammation reported following trauma (Chan et al. 2012). In particular, we observed a transient increase in circulating HMGB1 immediately post BH, which subsided within 48 hours. Similar trends have previously been reported in humans after blunt trauma not requiring admission to ICU (Giannoudis et al. 2010), but not after more severe trauma causing shock, in which case there is a transient peak within a few hours followed by elevated HMGB1 levels for prolonged periods (Peltz et al. 2009). HMGB1 is an alarmin present in nearly all cells that is passively secreted by necrotic or damaged cells and is actively secreted by monocytes, neutrophils and macrophages triggering the inflammatory cascade (Lotze et al. 2007). The immediate elevation of circulating HMGB-1 level post BH treatment suggests that this release is likely due to passive leakage from the fractionated tumor cell debris rather than active release by leukocytes – the mechanism that has been hypothesized in trauma patients (Peltz et al. 2009). In cancer, this passive release of HMGB1 from dying cancer cells following chemotherapy or radiotherapy was previously reported to potentiate TLR-4 expression in dendritic cells and consequently efficient processing and cross-presentation of antigens, and enhancement of effector immune response (Apetoh et al. 2007, Hato et al. 2014). Thus, it is encouraging that following BH a trend towards increased circulating HMGB1 was observed, although not reaching statistical significance most probably due to a limited sample size, and warrants further investigation of this effect within a larger cohort. The increased levels of other proinflammatory cytokines – TNF and IL-6 – were consistent with the known ability of HMGB-1 to amplify the production and secretion of proinflammatory mediators by monocytes (Andersson et al. 2000), and were sustained up to the 48-hour time point. At the same time, the levels of IL-10, which is a key anti-inflammatory cytokine were steadily increasing over the 48-hour time, indicating a shift towards inhibition of the systemic inflammatory processes.

Locally, the concentrations of both pro-inflammatory (TNF, IL-6 and IL-8) and anti-inflammatory (IL-10 and IL-13) cytokines in the BH-treated kidneys were increased compared to sham-treated control kidneys, suggesting the shifting balance between the inflammation and regulation processes. Interestingly, the levels of IFN-γ, which is primarily secreted by Th1 cells and stimulates cellular (as opposed to humoral) immunity, are significantly reduced in the BH-treated kidney. High levels of IFN-γ have been previously reported to contribute to acute and chronic kidney injury, and the suppression of IFN-γ in this context suggests that the inhibition processes may be ramped up to protect renal parenchymal tissue (Chung et al. 2011). Whether this regulation is only transient or chronic remains to be seen in experiments with more distant time points. Another important note is that the renal tissue cores were taken adjacent to, but not immediately from the BH-liquefied areas or control tumors. The cytokine levels in these benign kidney tissues may therefore not be immediately representative of the tumor or tumor lysate. In fact, the suppressed levels of IFN-γ in benign parenchyma may indicate that the IFN-γ -producing T-cells are preferentially recruited to the BH-treated tumor site.

In addition to investigating the cytokine milieu, we evaluated the immune infiltration of RCCs and benign kidney parenchyma by antigen-presenting cells – macrophages and dendritic cells – and T cells, both cytotoxic and regulatory, at the 48-hour time point. The major finding was enhanced infiltration of the CD8+ lymphocytes of not only BH-treated, but also contralateral RCC compared to sham-treated tumors. Conversely, no difference was observed in infiltration of dendritic cells or macrophages (both M1 and M2) between BH-treated and sham-treated kidneys. Taken together with the cytokine data above these findings suggest that by the 48-hour time point the course of processing of BH released tumor antigen and maturation of dendritic cells, T cell priming in the lymph nodes, and their subsequent migration to the tumor site may have already occurred. Indeed, the release of HMGB-1 that activates antigen-presenting cells was immediate and transient, and enhanced release of TNF and IL-6 secreted mostly by activated macrophages occurred within hours post treatment. This timeline is consistent with observations in other studies using mechanical fractionation of subcutaneously grafted tumors in mice by FUS or cryoablation (den Brok et al. 2006, Huang et al. 2012, Xing et al. 2008, Hoogenboom et al. 2015). In those studies tumor-infiltrating lymphocytes were not examined, but the increase in the number of activated, tumor antigen-specific dendritic cells in the draining lymph nodes was observed within 1–3 days following ablation. Similarly, in a study of molecular changes in healthy rat cardiac tissue following milder mechanical disruption by pulsed FUS (Jang et al. 2017), infiltrating macrophages and neutrophils were observed within the myocardium 24 hours post treatment, but were undetectable by 48 hours.

Multiple limitations of our study provide motivation for future experiments. First, the small number of animals per group limited the findings of statistically significant alterations in some of the outcome measures, although it did appear to capture trends and the overall dynamics of the immune response. Further studies with larger cohorts are required (and are currently underway) to rigorously describe the phenotype and activation status of the infiltrating T cells and antigen-presenting cells and to evaluate the immune response at more distant time points. In considering the clinical translation of this research, important limitations are the anatomic and physiological differences between our rat model system and

human patients. As mentioned above, we anticipate the difference in size between rat and human to be closely related to the acute safety outcomes of BH treatment, primarily in the incidence of bleeds and hematoma formation. Further, the accuracy of small animal tumor models in mimicking human disease has come under scrutiny in the past decade (Takao et al. 2015, Seok et al. 2013, Iannaccone and Jacob 2009), with particular focus on the use of rapidly growing subcutaneously grafted mouse tumor models which are not always representative of the tumor defense mechanisms and resulting immune tolerance. Thus, a strength of this work is the use of the Eker rat model, in which rats have an intact immune system and develop slowly growing bilateral RCCs with similar biology and behavior to small human RCC (Liu et al. 2003, Habib et al. 2011, Kenerson et al. 2002). Additionally, because the tumors are *de novo*, their blood supply and tumor microenvironment is more similar to human disease. However, even with these factors in mind, care must be taken when extrapolating characteristics of the systemic and local immune responses to BH treatment of Eker rat RCC to humans.

CONCLUSIONS

Non-invasive BH-induced fractionation of *de novo* RCC was feasible and well tolerated in the Eker rat model. BH-induced activation of immune responses within 48 hours suggest that both inflammatory and regulatory cascades are triggered systemically and locally in adjacent renal tissues, reminiscent of the acute inflammatory/immunological responses observed in trauma. The enhanced infiltration of both treated and contralateral RCCs by CD8+ T cells and transient release of pro-inflammatory cytokines at both local and systemic level suggests activation of systemic anti-tumor immune response(s), which warrants further investigation of BH in the context of enhancing anti-tumor immunity.

Supplementary Material

Refer to Web version on PubMed Central for supplementary material.

ACKNOWLEDGEMENTS

This work was supported by U.S. National Institute of Biomedical Imaging and Bioengineering grant K01EB015745, and grant funding from the Urology Care Foundation and Focused Ultrasound Foundation. We gratefully acknowledge Drs. Raymond Yeung and Heidi Kenerson for providing the Eker rats for this study and the University of Washington Histology and Imaging Core for performing immunohistochemistry staining.

REFERENCES

Andersson U, Wang H, Palmblad K, Aveberger AC, Bloom O, Erlandsson-Harris H, Janson A, Kokkola R, Zhang M, Yang H, Tracey KJ. High mobility group 1 protein (HMG-1) stimulates proinflammatory cytokine synthesis in human monocytes. J Exp Med. 2000;192(4):565–570. [PubMed: 10952726]

Apetoh L, Ghiringhelli F, Tesniere A, Obeid M, Ortiz C, Criollo A, Mignot G, Maiuri MC, Ullrich E, Saulnier P, Yang H, Amigorena S, Ryffel B, Barrat FJ, Saftig P, Levi F, Lidereau R, Nogues C, Mira JP, Chompret A, Joulin V, Clavel-Chapelon F, Bourhis J, André F, Delaloge S, Tursz T, Kroemer G, Zitvogel L. Toll-like receptor 4-dependent contribution of the immune system to anticancer chemotherapy and radiotherapy. Nat Med. 2007;13(9):1050–1059. [PubMed: 17704786]

Campbell SC, Novick AC, Belldegrun A, Blute ML, Chow GK, Derweesh IH, Faraday MM, Kaouk JH, Leveillee RJ, Matin SF, Russo P, Uzzo RG; Practice Guidelines Committee of the American

Urological Association. Guideline for management of the clinical T1 renal mass. J Urol. 2009 10;182(4):1271–9. [PubMed: 19683266]

Chan JK, Roth J, Oppenheim JJ, Tracey KJ, Vogl T, Feldmann M, Horwood N, Nanchahal J. Alarmins: awaiting a clinical response. J Clin Invest. 2012;122(8):2711–2719. [PubMed: 22850880]

Chevillet JR, Khokhlova TD, Giraldez MD, Schade GR, Starr F, Wang YN, Gallichotte EN, Wang K, Hwang JH, Tewari M. Release of Cell-free MicroRNA Tumor Biomarkers into the Blood Circulation with Pulsed Focused Ultrasound: A Noninvasive, Anatomically Localized, Molecular Liquid Biopsy. Radiology. 2017; 283(1):158–167. [PubMed: 27802108]

Chen GY, Nunez G. Sterile inflammation: sensing and reacting to damage. Nat Rev Immunol. 2010;10(12):826–837. [PubMed: 21088683]

Chung AC, Lan HY. Chemokines in renal injury. J Am Soc Nephrol. 2011;22(5):802–809. [PubMed: 21474561]

den Brok MH, Sutmuller RP, Nierkens S, Bennink EJ, Frielink C, Toonen LW, Boerman OC, Figdor CG, Ruers TJ, Adema GJ. Efficient loading of dendritic cells following cryo and radiofrequency ablation in combination with immune modulation induces anti-tumour immunity. Br J Cancer. 2006;95(7):896–905. [PubMed: 16953240]

Draube A, Klein-González N, Mattheus S, Brillant C, Hellmich M, Engert A, von Bergwelt-Baildon M Dendritic cell based tumor vaccination in prostate and renal cell cancer: a systematic review and meta-analysis. PLoS One. 2011;6(4):e18801. [PubMed: 21533099]

Giannoudis PV, Mallina R, Harwood P, Perry S, Sante ED, Pape HC. Pattern of release and relationship between HMGB-1 and IL-6 following blunt trauma. Injury. 2010;41(12):1323–1327. [PubMed: 20887988]

Habib SL, Yadav A, Mahimainathan L, Valente AJ. Regulation of PI 3-K, PTEN, p53, and mTOR in Malignant and Benign Tumors Deficient in Tuberin. Genes Cancer. 2011;2(11):1051–1060. [PubMed: 22737271]

Hall TL, Hempel CR, Wojno K, Xu Z, Cain CA, Roberts WW. Histotripsy of the prostate: dose effects in a chronic canine model. Urology. 2009;74(4):932–937. [PubMed: 19628261]

Hato SV, Khong A, de Vries IJ, Lesterhuis WJ. Molecular pathways: the immunogenic effects of platinum-based chemotherapeutics. Clin Cancer Res. 2014;20(11):2831–2837. [PubMed: 24879823]

Hoogenboom M, Eikelenboom D, den Brok MH, Veltien A, Wassink M, Wesseling P, Dumont E, Fütterer JJ, Adema GJ, Heerschap A. In vivo MR guided boiling histotripsy in a mouse tumor model evaluated by MRI and histopathology. NMR Biomed. 2016;29(6):721–731. [PubMed: 27061290]

Hoogenboom M, Eikelenboom D, den Brok MH, Heerschap A, Futterer JJ, Adema GJ. Mechanical high-intensity focused ultrasound destruction of soft tissue: working mechanisms and physiologic effects. Ultrasound Med Biol. 2015;41(6):1500–1517. [PubMed: 25813532]

Hu Z, Yang XY, Liu Y, Sankin GN, Pua EC, Morse MA, Lyerly HK, Clay TM, Zhong P. Investigation of HIFU-induced anti-tumor immunity in a murine tumor model. J Transl Med. 2007;5:34. [PubMed: 17625013]

Huang X, Yuan F, Liang M, Lo HW, Shinohara ML, Robertson C, Zhong P. M-HIFU inhibits tumor growth, suppresses STAT3 activity and enhances tumor specific immunity in a transplant tumor model of prostate cancer. PLoS One. 2012;7(7):e41632. [PubMed: 22911830]

Humphreys BD, Valerius MT, Kobayashi A, Mugford JW, Soeung S, Duffield JS, McMahon AP, Bonventre JV. Intrinsic epithelial cells repair the kidney after injury. Cell Stem Cell. 2008;2(3): 284–291. [PubMed: 18371453]

Iannaccone PM, Jacob HJ. Rats! Dis Model Mech. 2009;2(5–6):206–210 [PubMed: 19407324]

Jang KW, Tu T-W, Nagle ME, Lewis BK, Burks SR, Frank JA. Molecular and histological effects of MR-guided pulsed focused ultrasound to the rat heart. J. Transl. Med 2017;15:252. [PubMed: 29237455]

Kenerson HL, Aicher LD, True LD, Yeung RS. Activated mammalian target of rapamycin pathway in the pathogenesis of tuberous sclerosis complex renal tumors. Cancer Res. 2002;62(20):5645–5650. [PubMed: 12384518]

Khokhlova TD, Canney MS, Khokhlova VA, Sapozhnikov OA, Crum LA, Bailey MR. Controlled tissue emulsification produced by high intensity focused ultrasound shock waves and millisecond boiling. J Acoust Soc Am. 2011;130(5):3498–3510. [PubMed: 22088025]

Khokhlova TD, Wang YN, Simon JC, Cunitz BW, Starr F, Paun M, Crum LA, Bailey MR, Khokhlova VA. Ultrasound-guided tissue fractionation by high intensity focused ultrasound in an in vivo porcine liver model. Proc Natl Acad Sci U S A. 2014;111(22):8161–8166. [PubMed: 24843132]

Khokhlova V, Schade G, Khokhlova T, Wang YN, Simon J, Starr F, Bailey M, Kreider W Pilot in vivo studies on transcutaneous boiling histotripsy in porcine liver and kidney. The Journal of the Acoustical Society of America. 2016;140(4):3030–3030.

Khokhlova VA, Fowlkes JB, Roberts WW, Schade GR, Xu Z, Khokhlova TD, Hall TL, Maxwell AD, Wang YN, Cain CA. Histotripsy methods in mechanical disintegration of tissue: towards clinical applications. Int J Hyperthermia. 2015;31(2):145–162. [PubMed: 25707817]

Klune JR, Dhupar R, Cardinal J, Billiar TR, Tsung A. HMGB1: endogenous danger signaling. Mol Med. 2008;14(7–8):476–484. [PubMed: 18431461]

Kroeze SG, van Melick HH, Nijkamp MW, Kruse FK, Kruijssen LW, van Diest PJ, Bosch JL, Jans JJ. Incomplete thermal ablation stimulates proliferation of residual renal carcinoma cells in a translational murine model. BJU Int. 2012 9;110(6 Pt B):E281–6. [PubMed: 22612555]

Liu MY, Poellinger L, Walker CL. Up-regulation of hypoxia-inducible factor 2alpha in renal cell carcinoma associated with loss of Tsc-2 tumor suppressor gene. Cancer Res. 2003;63(10):2675–2680. [PubMed: 12750296]

Lotze MT, Zeh HJ, Rubartelli A, Sparvero LJ, Amoscato AA, Washburn NR, Devera ME, Liang X, Tör M, Billiar T. The grateful dead: damage-associated molecular pattern molecules and reduction/oxidation regulate immunity. Immunol Rev. 2007;220:60–81. [PubMed: 17979840]

McDermott DF, Drake CG, Sznol M, Choueiri TK, Powderly JD, Smith DC, Brahmer JR, Carvajal RD, Hammers HJ, Puzanov I, Hodi FS, Kluger HM, Topalian SL, Pardoll DM, Wigginton JM, Kollia GD, Gupta A, McDonald D, Sankar V, Sosman JA, Atkins MB. Survival, Durable Response, and Long-Term Safety in Patients With Previously Treated Advanced Renal Cell Carcinoma Receiving Nivolumab. J Clin Oncol. 2015;33(18):2013–2020. [PubMed: 25800770]

McDorman KS, Wolf DC. Use of the spontaneous Tsc2 knockout (Eker) rat model of hereditary renal cell carcinoma for the study of renal carcinogens. Toxicol Pathol. 2002;30(6):675–680. [PubMed: 12512868]

Parsons JE, Cain CA, Abrams GD, Fowlkes JB. Pulsed cavitational ultrasound therapy for controlled tissue homogenization. Ultrasound Med Biol. 2006;32(1):115–129. [PubMed: 16364803]

Peltz ED, Moore EE, Eckels PC, Damle SS, Tsuruta Y, Johnson JL, Sauaia A, Silliman CC, Banerjee A, Abraham E. Hmgb1 Is Markedly Elevated within 6 Hours of Mechanical Trauma in Humans. Shock. 2009;32(1):17–22. [PubMed: 19533845]

Seok J, Warren HS, Cuenca AG, Mindrinos MN, Baker HV, Xu W, Richards DR, McDonald-Smith GP, Gao H, Hennessy L, Finnerty CC, López CM, Honari S, Moore EE, Minei JP, Cuschieri J, Bankey PE, Johnson JL, Sperry J, Nathens AB, Billiar TR, West MA, Jeschke MG, Klein MB, Gamelli RL, Gibran NS, Brownstein BH, Miller-Graziano C, Calvano SE, Mason PH, Cobb JP, Rahme LG, Lowry SF, Maier RV, Moldawer LL, Herndon DN, Davis RW, Xiao W, Tompkins RG; Inflammation and Host Response to Injury, Large Scale Collaborative Research Program. Genomic responses in mouse models poorly mimic human inflammatory diseases. Proc Natl Acad Sci U S A. 2013;110(9):3507–3512. [PubMed: 23401516]

Simon JC, Sapozhnikov OA, Khokhlova VA, Wang YN, Crum LA, Bailey MR. Ultrasonic atomization of tissue and its role in tissue fractionation by high intensity focused ultrasound. Phys Med Biol. 2012;57(23):8061–8078. [PubMed: 23159812]

Takao K, Miyakawa T. Genomic responses in mouse models greatly mimic human inflammatory diseases. Proc Natl Acad Sci U S A. 2015;112(4):1167–1172. [PubMed: 25092317]

Venkatesan AM, Wood BJ, Gervais DA. Percutaneous ablation in the kidney. Radiology. 2011;261(2):375–391. [PubMed: 22012904]

Wang YN, Khokhlova T, Bailey M, Hwang JH, Khokhlova V. Histological and biochemical analysis of mechanical and thermal bioeffects in boiling histotripsy lesions induced by high intensity focused ultrasound. Ultrasound Med Biol. 2013;39(3):424–438. [PubMed: 23312958]

Waynforth HB, Roe GM. The Eker renal tumor rat. General immune status in relation to a varying tumor burden. Neoplasma. 1981;28(6):697–703. [PubMed: 7040995]

Xing Y, Lu X, Pua EC, Zhong P. The effect of high intensity focused ultrasound treatment on metastases in a murine melanoma model. Biochem Biophys Res Commun. 2008;375(4):645–650. [PubMed: 18727919]

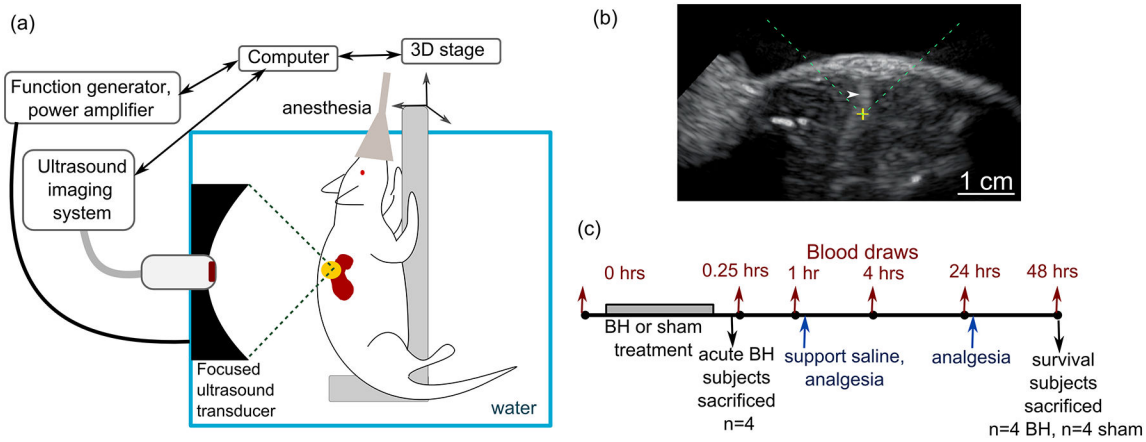

Figure 1.

(a) Schematic diagram of the experimental setup for ultrasound-guided boiling histotripsy (BH) ablation of renal tumors in Eker rats. **(b)** An example of B-mode ultrasound image during BH treatment. The position of the focused ultrasound (FUS) transducer focus is indicated on the screen as a yellow cross; the FUS beam is incident from the top of the image (dashed green lines). The transient elongated hyperechoic region (white arrowhead) that appears after each BH pulse corresponds to highly reflective vapor bubbles. **(c)** Timeline of the experimental procedures.

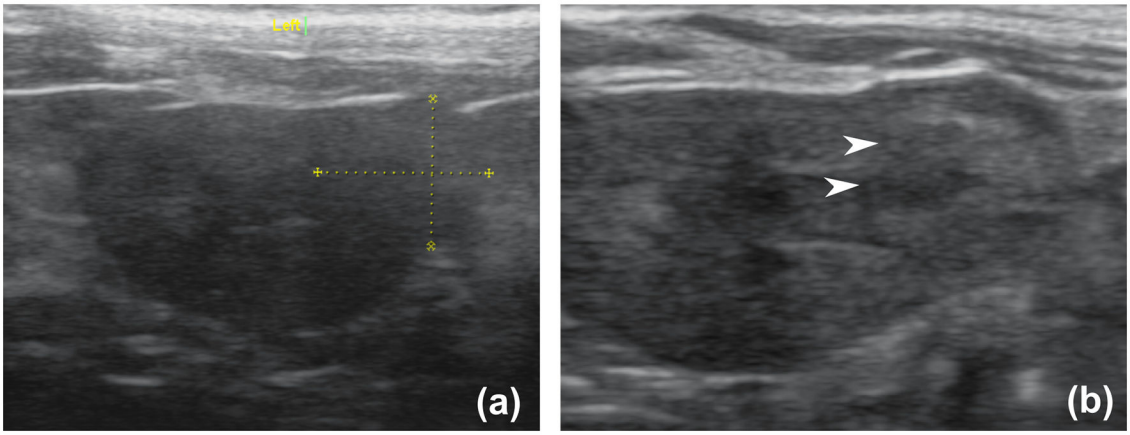

Figure 2.

A representative set of high resolution ultrasound images of the rat RCC before **(a)** and a few minutes after **(b)** BH treatment. The white arrowheads indicate the area of hypoechogenicity post treatment.

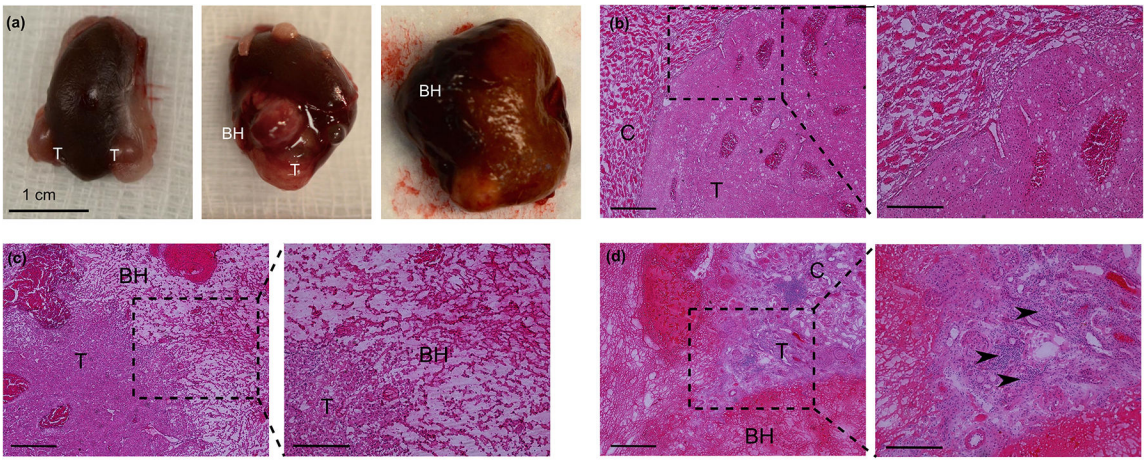

Figure 3.

(a) Gross view of RCC (T) from sham (left) and BH-treated subjects at 1 hour (center) and 48 hours (right) time points. **(b)** Representative histological appearance of a sham-treated renal tumor (T) and adjacent kidney cortex (C). **(c)** Histological appearance of the BH-treated tumor at 1 hour time point reveals a sharp boundary between homogenized (BH) and intact tumor (T). **(d)** Histological appearance of BH-treated tumor at 48 hour time point. Acute inflammatory infiltrate is apparent on higher magnification (inset, arrowheads).

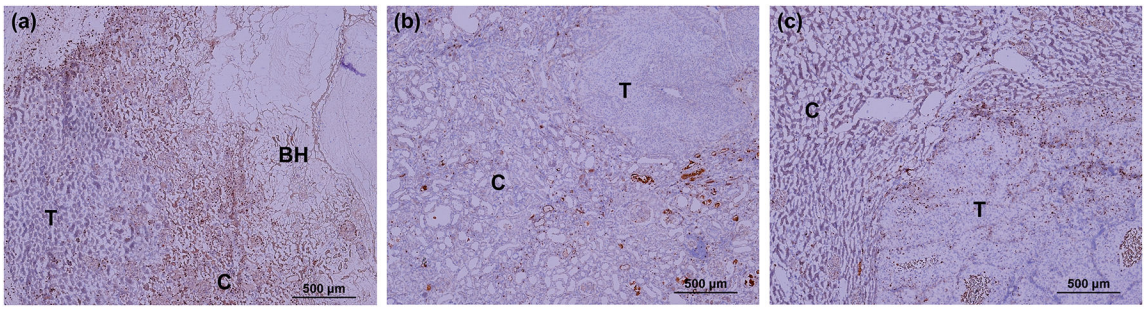

Figure 4.

IHC sections of kidneys stained for proliferation marker Ki67 (brown stain) at 48 hour time point. **(a)** The border between BH-treated lesion (BH), benign renal cortex (C) and tumor (T). Enhanced nuclear staining indicating proliferation in a narrow rim around the BH cavity in benign cortex, but not in tumor tissue. **(b)** A distant, untreated tumor in the same kidney as (a) with surrounding cortex showing the lack of staining in the tumor. **(c)** Sham-treated tumor showing the background level of staining.

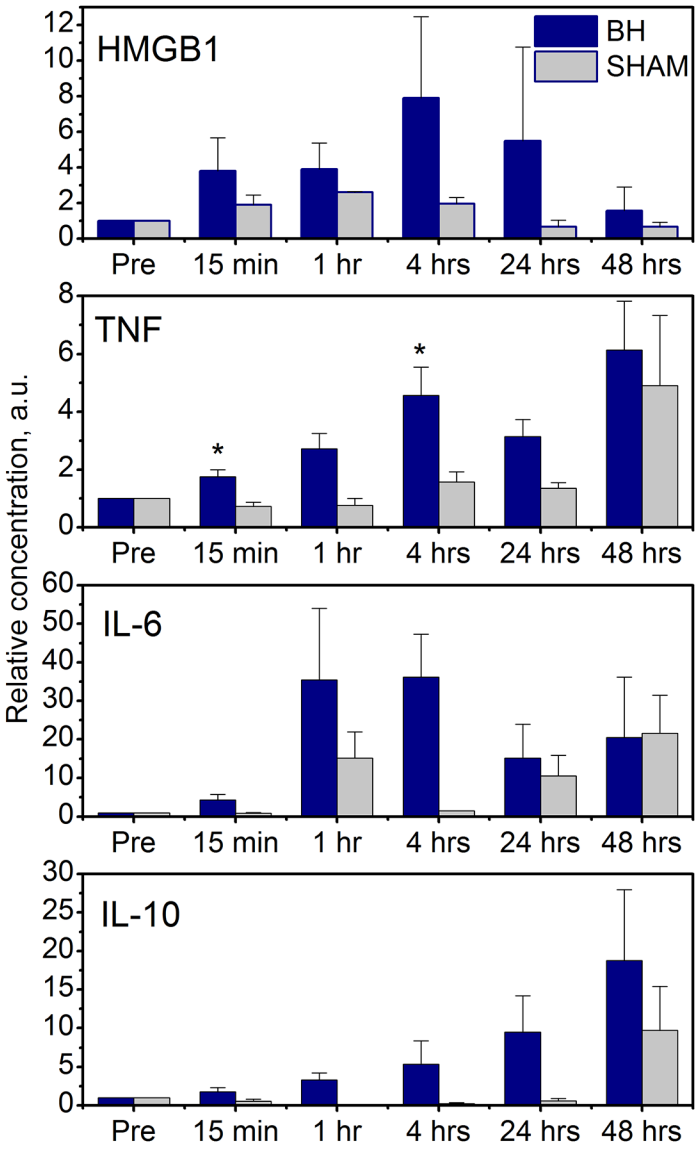

Figure 5.

Dynamics of circulating plasma cytokines over the course of 48 hours post BH (purple bars) and sham (grey bars) treatment (n=4/group). Error bars represent standard error. All levels are normalized to the pre-treatment level ("Pre"). * $p<0.05$

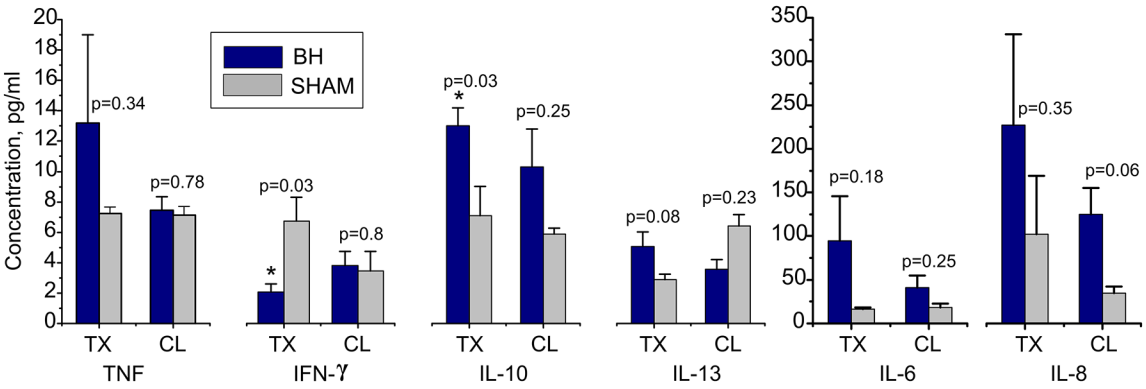

Figure 6.

Intrarenal cytokine levels in the kidneys of BH-treated (purple bars) and sham-treated (light grey) subjects. The error bars represent standard error. P values are listed separately for treated and contralateral kidneys vs sham treated controls (n=4/group). TX – treated kidney, CL – contralateral kidney.

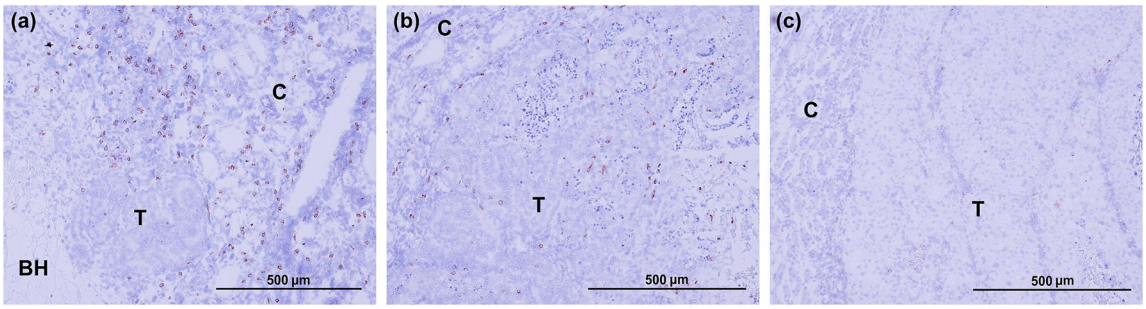

Figure 7.

IHC staining for CD8+ cells (brown stain) reveal enhanced infiltration of CD8+ cells in both BH-treated **(a)** and contralateral **(b)** tumors, but not in sham-treated tumors **(c)** at 48 hour time point.